Chapter 5

Mode Transition and Hysteresis in Inductively Coupled Plasma Sources

Shu-Xia Zhao

Additional information is available at the end of the chapter

http://dx.doi.org/10.5772/intechopen.76654

Abstract

In this chapter, the characteristics of low-temperature inductively coupled plasma sources, that is, non-equilibrium, weakly ionized and bounded plasma, are described. The phenomenon of mode transition and hysteresis is one of the main physics aspects that happens in this source. Via a hybrid model, the behaviors of plasma parameters, electron kinetics and neutral species during mode transition are presented. Still, the role of metastables and multistep ionization on triggering the hysteresis is investigated. Using a fluid model that couples the equivalent circuit module, the discontinuity of mode transition and hysteresis are observed by tuning the matching network impedance. The work indicates the mutual interaction between the plasma and the circuit excites hysteresis. Besides these findings, the other important aspects of this phenomenon are briefly discussed. To the author, the exploration on the precursors that trigger hysteresis is the most attractive topic. The investigations advance the improvement of analytical theory, numerical modeling and experimental diagnostics of low-temperature plasma physics.

Keywords: low-temperature plasma, inductively coupled plasma, mode transition and hysteresis, hybrid model, fluid model, equivalent circuit, multistep ionizations

1. Introduction

The inductively coupled plasma (ICP) source is one of the most important low-temperature plasma sources that find widespread applications in many fields [1], such as plasma photonic crystals, synthesis of nanomaterials and nanostructured materials, atomic layer processing, agriculture and innovative food cycles, medicines, environments, plasma-assisted combustion and chemical conversion and aerospace application (propulsion and flow control) and so on. Driven within the domains of radio frequency electromagnetic and rather low-pressure

(~mTorrs) ranges, the ICP sources present several advantages, such as high-plasma density, high anisotropy in the sheath, independent control of incident flux density and energy and simple low-cost reactor configuration (unwanted for the static magnetic devices) over some other plasma sources, such as capacitively coupled plasma and electron cyclotron resonance reactor [2]. As compared to the atmospheric discharges, this sort of low-pressure radio frequency plasma sources are known for their non-equilibrium properties, that is, $T_e \gg T_i > T_n$, where T_e, T_i and T_n are temperatures of electrons, ions and neutrals, respectively [3], due to the low-temperature peculiarity of this type of plasma source. Another essential feature is its weak ionization degree that ensures the abundance of collisions and reactions between charged species and neutrals, which is quite different with the high-temperature fully ionized plasmas where only the Coulomb interactions between charged species are important [4]. Of great importance is the diversity in the mutual interactions among charged and neutral species, which are classified into elastic and inelastic collisions with respect to the principle of kinetic energy balance. Regarding species specialty and colliding outcomes, the inelastic collisions can be described as type (1) ionization, dissociation, electronic, rotational, vibrational excitation, attachment, detachment and de–excitation, which mainly occur between electrons and neutrals; type (2) recombination, associations, charge exchange, excitation transfer and penning ionizations, which mainly happen among heavy species (meant to all species except for electrons); and type (3) the spontaneous radiation from excited state species (without a trigger) [5]. The elastic scattering to some extent determines plasma transport process and hence spatial characteristics of plasma via the parameter of momentum transfer collision frequency, while the inelastic collisions that sustain the weakly ionized plasma mainly determine the energy loss mechanism and give steady-state plasma components optical emission. Finally, all low-temperature plasma sources are generated in chambers with their respective fixed configurations and more importantly with limit space dimension. This means that all the plasmas are bounded plasmas, as compared with the space plasma; therefore, the sheath, produced on all bound surfaces, forms one important constituent of low-temperature plasma physics [6]. In a word, non-equilibrium, weak ionization and plasma bounds characterize the low-pressure radio frequency plasma source as complicated and multi-disciplinary.

Even with the above complexity, rich and fruitful interesting physics phenomena and mechanisms are already revealed in these low-pressure and radio frequency plasma sources via present efforts. In particular, in the ICP sources, pulsed radio frequency power source [7], standing wave effects [8], nonlinear harmonics [9], double coil discharges [10], anomalous skin effects [11], nonlocal electron kinetics [12], mode transition and hysteresis [13] and so on are still or have been hot research frontiers that draw attention. In this chapter, the mode transitions and hysteresis topic is focused upon. This topic has been historically studied well and continually occupies people's attention due to its complexity of the multi-factor interactions and potential application in achieving stable plasma sources for the processing technique. The ICP source is famous for its capacity of operating at two different modes, that is, capacitive and inductive modes. The capacitive mode is sustained by radial and axial electromagnetic fields, analogous to conventional capacitively coupled plasma source that is excited by the electrostatic field and hence is abbreviated as the E mode. The inductive mode is sustained by the azimuthal electromagnetic field caused by coil current and is abbreviated as H mode. Remember that the

power source applied to the coil is temporally varied in the range of radio frequency. At low-coil power, the ICP source is maintained at E mode, where the plasma density and optical emissions are weak, and the glow area of discharge is more localized under the coil. As we increase the coil power, the discharge transfers abruptly or smoothly toward H mode, where the plasma density and current are significantly increased and the optical emission is strengthened. Moreover, the discharge is more uniform. Interestingly, at certain circumstances, when cycling the power source, the trajectories of plasma parameters versus upward and downward powers don't coincide; hence, hysteresis is formed and the ICP source is therefore famous for its other feature, that is, the existence of two stable states at one fixed power value. In labs of academia or enterprise, the ICP sources are triggered from the E mode at the beginning and then transferred to H mode. Most of the plasma processing techniques prefer to be conducted in the H mode due to its better plasma properties. Therefore, understanding the E–H mode transition and hysteresis is very meaningful to the related industry.

This chapter is outlined as follows. In Section 2, the major achievements of the author on this topic are presented. Three subtopics and the used methodology are discussed and described, aimed at demonstrating to readers the characteristics of plasma parameters, electron kinetics and neutral species during mode transition and excitation of discontinuous mode transition and hysteresis by the external circuit. Finally, the conclusion and further remarks are given in Section 3.

2. Theoretical and experimental investigations of mode transitions and hysteresis: An overview

2.1. Characteristics of basic plasma parameters

In this part, the characteristics of electron parameters, density, temperature and energy distribution function and plasma potential at two modes are presented via the two-dimensional hybrid model [14]. The hybrid model consists of three parts, that is, fluid module, electron Monte Carlo module and electromagnetic module. Species density and momentum, together with the electrostatic field generated by net charge density (analogous to ambipolar diffusion field), are given by the fluid module. Electron transport and collision coefficients, and the effective electron temperature, are calculated through the Monte Carlo method and then transferred to the fluid module. The electromagnetic module calculates the electromagnetic field generated via the coil current and voltage through the Maxwellian's equations, based on the electron conductivity from the fluid module. Both the electrostatic and electromagnetic fields are sent to the Monte Carlo module to push the electrons via Newton's law. The interactions of three modules are illustrated by the model flowchart in **Figure 1**. The three modules are iterated with each other until a final steady state is achieved. In this chapter, a cylindrical inductively coupled plasma reactor with planar coil is used, as shown in **Figure 2**.

In **Figures 3** and **4**, the calculated electron density and temperature profiles versus coil current at the pressure of 20 mTorr are presented. In **Figure 3**, at low-coil current, 10 A, the density

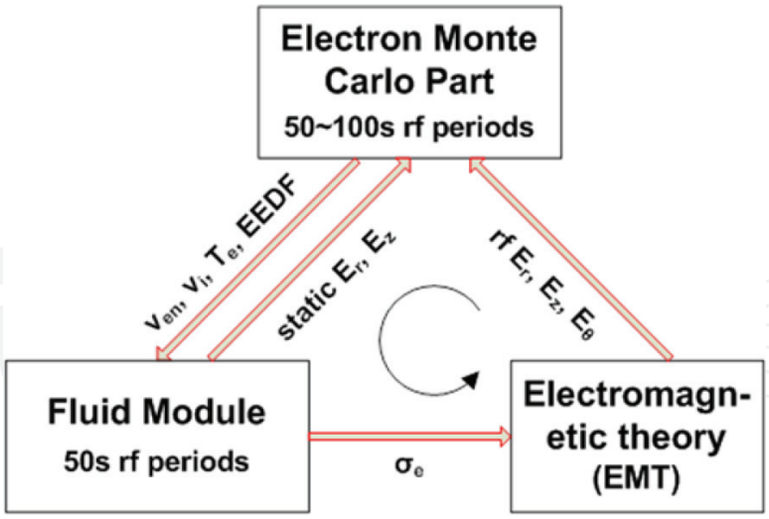

Figure 1. Flowchart of the hybrid model.

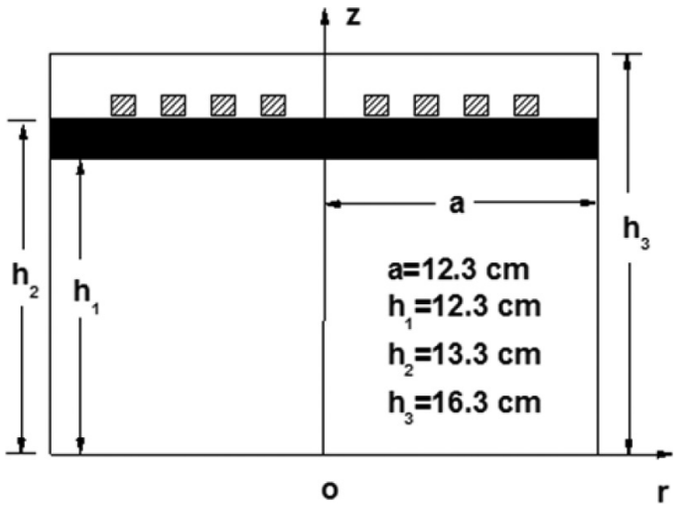

Figure 2. Schematic of the cylindrical inductively coupled discharge configuration.

magnitude is low and the profile is smooth. At high coil current, 40 A, the density magnitude is high, more or less four factors higher than the 10 A case. Meanwhile, the density is peaked under the coil, as referred to the reactor in **Figure 2**. The E–H mode transition happened along with increase in the coil current. In **Figure 4**, at E mode, that is, 10 A, the electron temperature is high around the plasma chamber bound but sinks at the discharge center region. This is because the ambipolar diffusion potential barrier suppresses the electrons from entering the sheath for heating due to the lack of elastic collisions at low pressure. As known, this is a representative feature for the capacitive discharges [15]. At the H mode, that is, 40 A, the temperature profile is substantially changed. It peaks under the coil and more or less decreases toward the center, bottom and sidewall. Besides, the sink area of the temperature profile is significantly shrunk and moves toward the coil, as compared to the E mode. The appearance of temperature sink at different coil currents and its alteration with coil current is related to the

http://dx.doi.org/10.5772/intechopen.76654

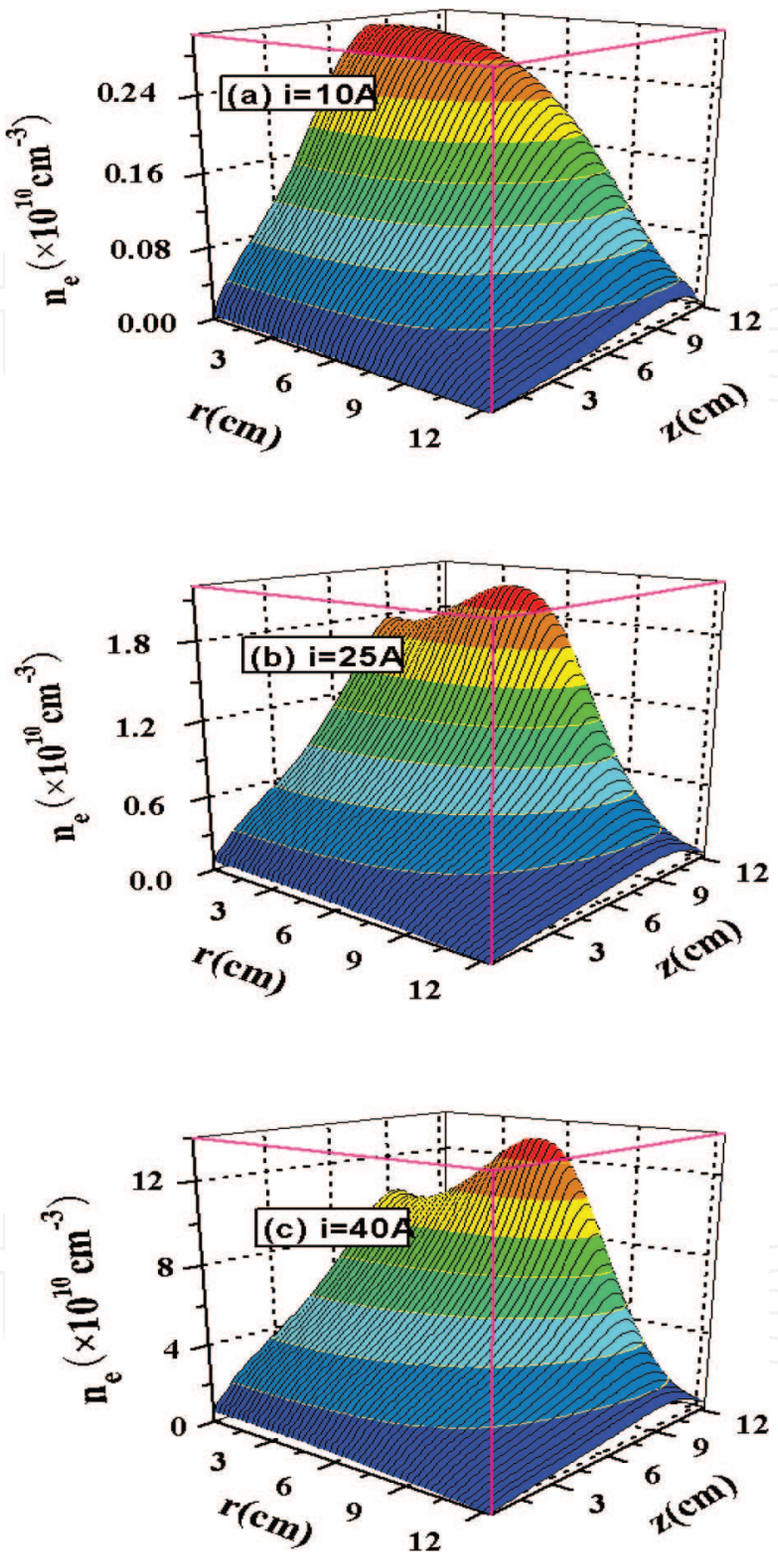

Figure 3. Electron density n_e profile versus coil current at the pressure of 20 mTorr.

spatial potential distribution in **Figure 5**, where the potential barrier is shifted from the discharge center to the coil with the coil current and meanwhile the area of potential barrier is decreased.

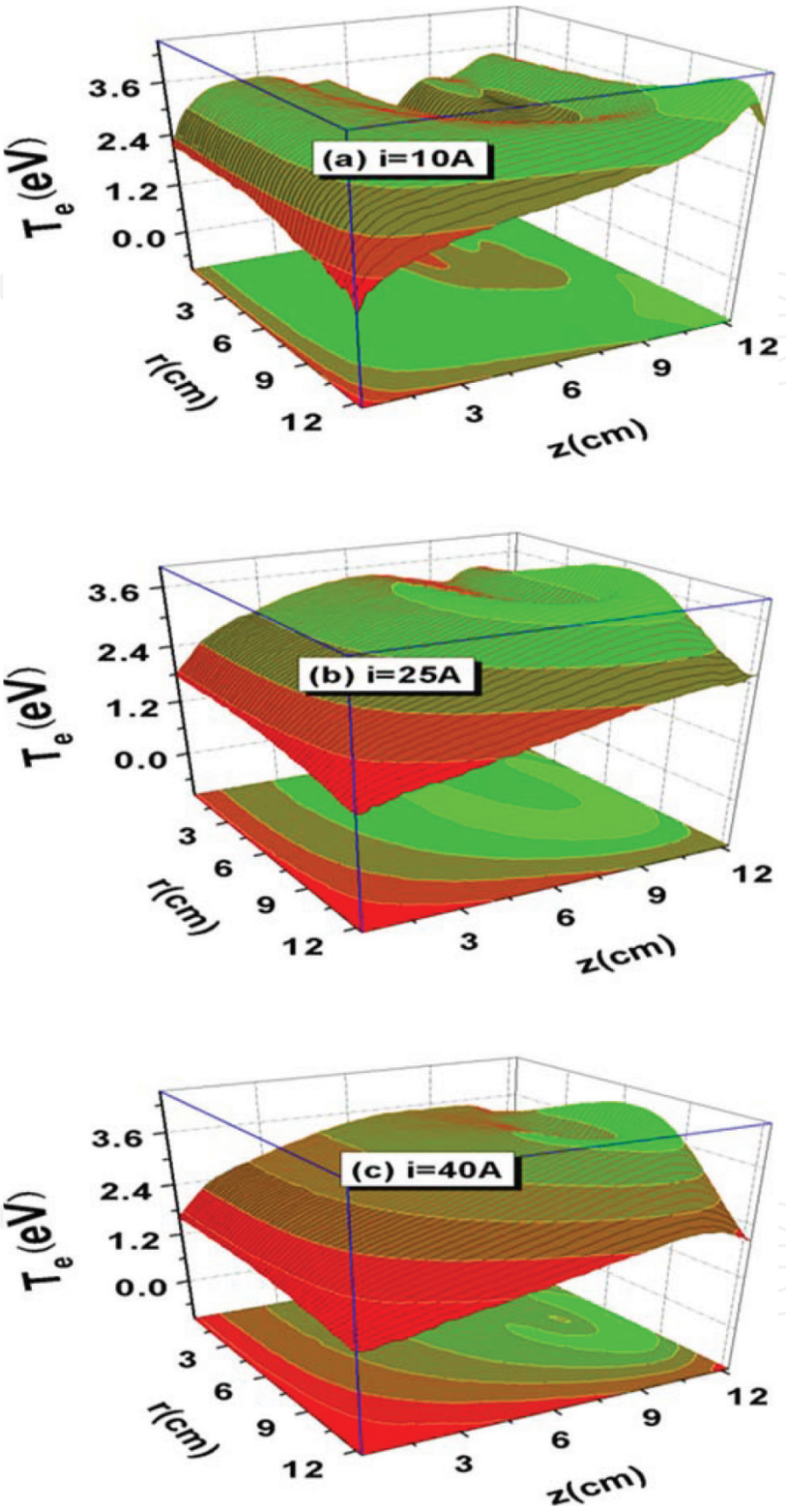

Figure 4. Electron temperature T_e profile versus coil current at the pressure of 20 mTorr.

In **Figure 6**, the electron energy distribution functions (EEDFs) of E and H modes, sampled at the discharge center, are compared at different pressures. At low pressure, that is, 20 mTorr, a prominent low-energy peak is found in the EEDF of the E mode due to the suppression of

http://dx.doi.org/10.5772/intechopen.76654

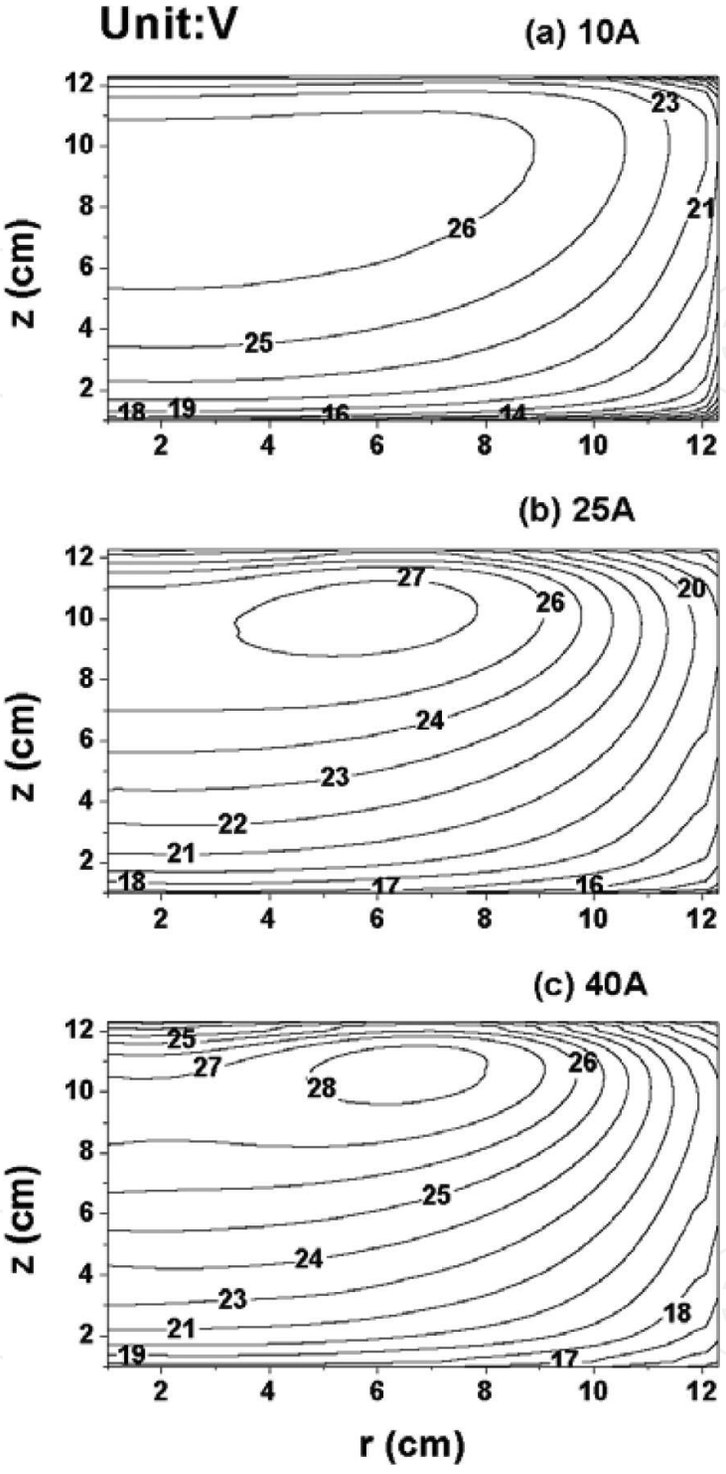

Figure 5. Plasma potential profile versus coil current at the pressure of 20 mTorr.

potential barrier, and it disappears at H mode because the barrier shifts toward the coil. At high pressures, that is, 50 and 100 mTorr, the EEDFs evolve to an opposite way, that is, low-energy electrons' amount of the H mode is higher than the E mode. This is because at high pressures the suppression of the potential barrier is not important anymore due to the frequent elastic collisions between electrons and neutrals at high electron densities. Hence in the electron

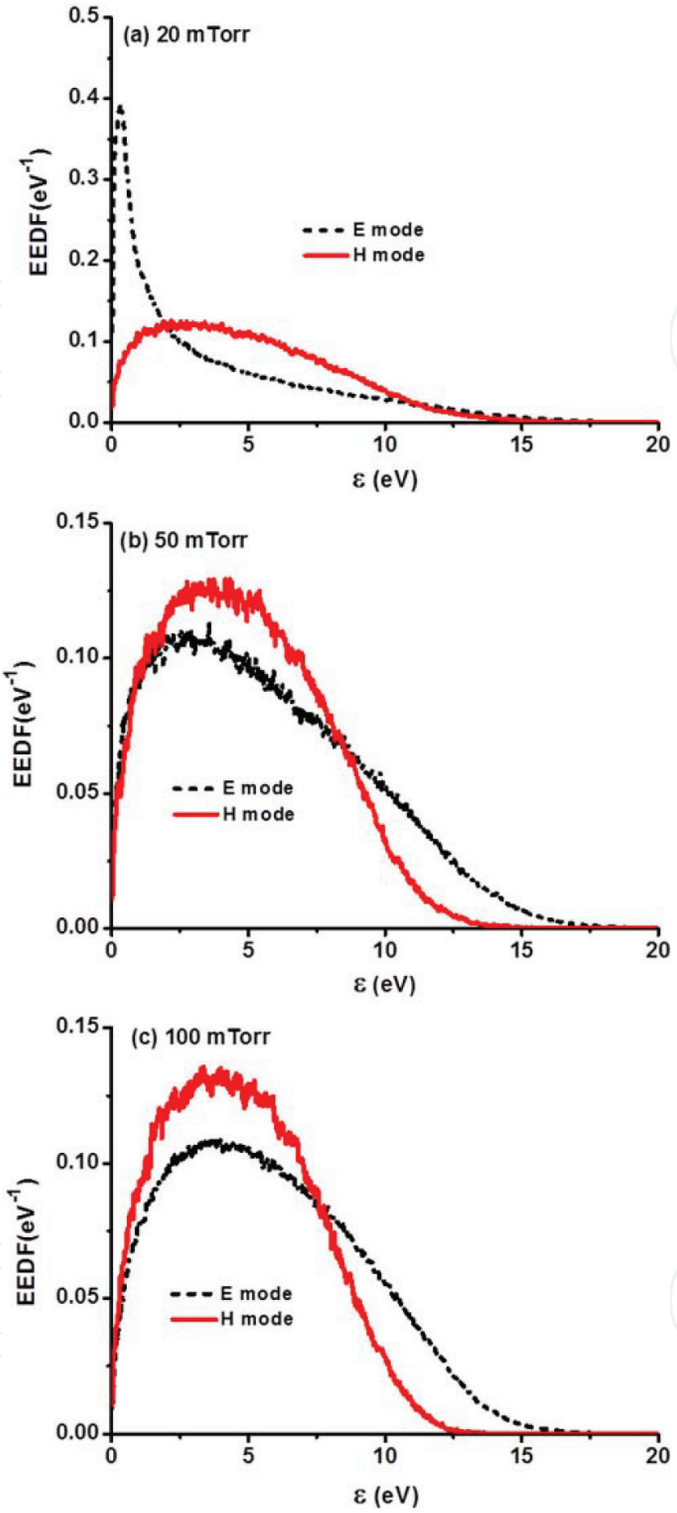

Figure 6. Comparisons of electron energy distribution function (EEDF) of E and H modes at different pressures. The EEDFs are sampled at the discharge center.

temperature profile (see **Figure 7**), the sink region disappears. The temperature profiles of E and H mode are representative of the capacitive and inductive discharges, and, as is well known, the temperature value in the E mode is higher than in the H mode [16]. To demonstrate the electron kinetics better, in **Figure 8**, the electron energy probability function (EEPF) variation with coil

http://dx.doi.org/10.5772/intechopen.76654

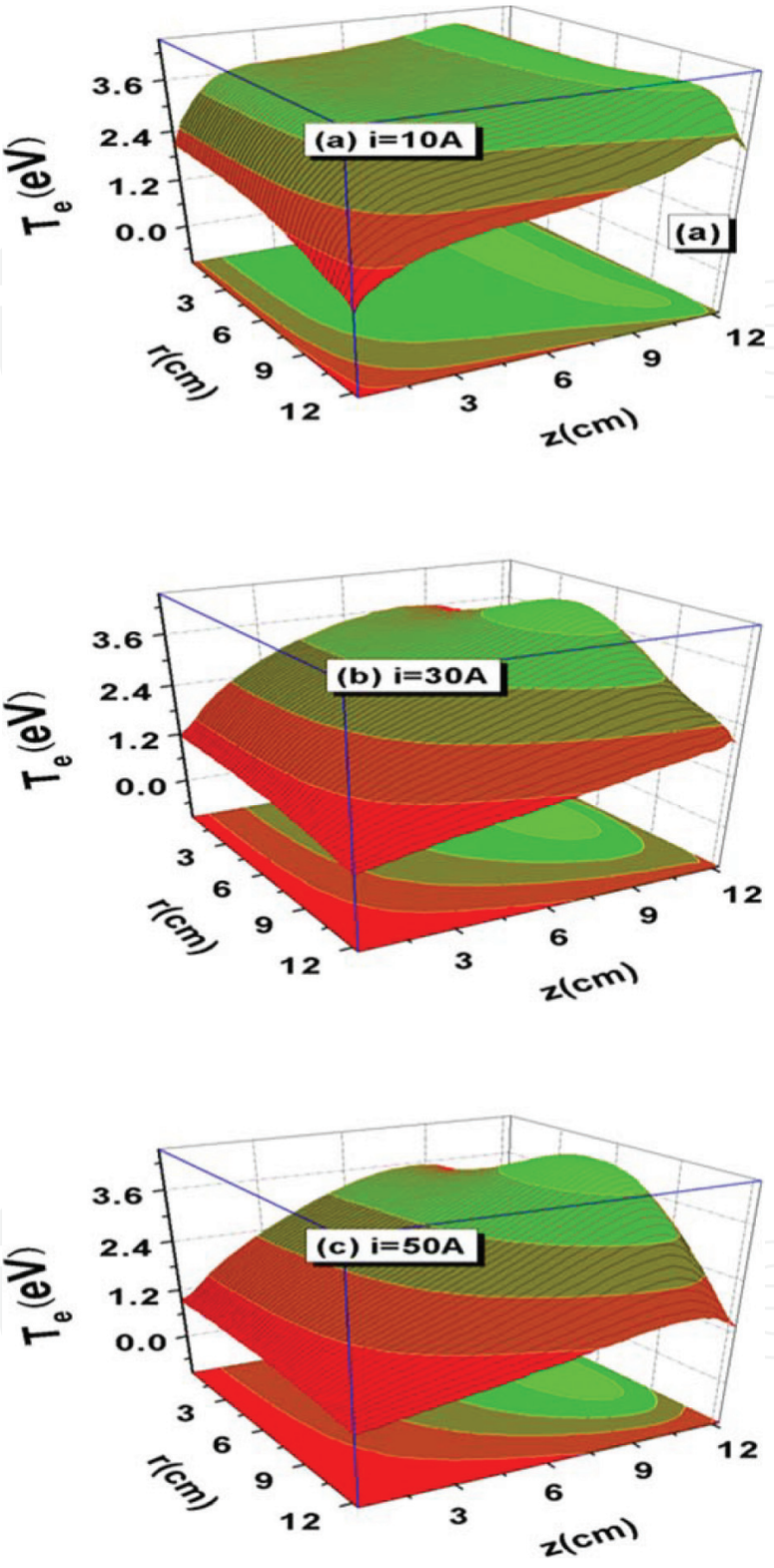

Figure 7. Electron temperature T_e profile versus coil current at the pressure of 100 mTorr.

current at low pressure of 20 mTorr is shown. Clearly, at the E mode, that is, with the coil current less than and equal to 20 A, the obvious three-temperature Maxwellian distribution is observed. The low-energy electron peak, as mentioned before, is formed by the suppression of the potential

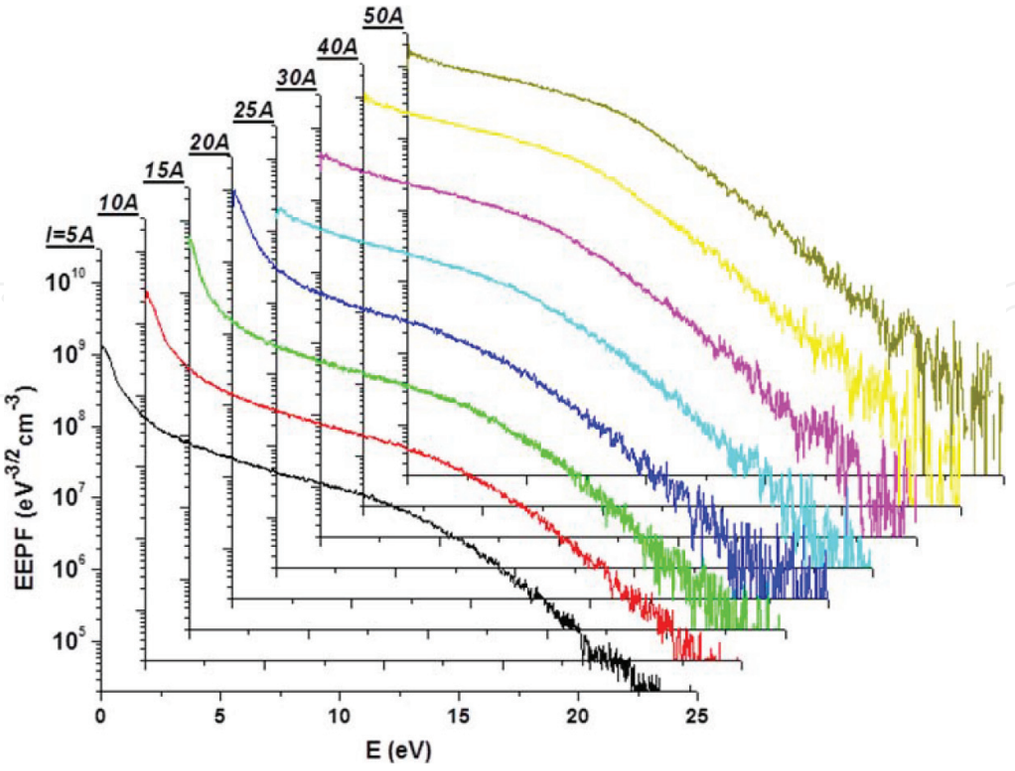

Figure 8. Evolution of electron energy probability (EEPF) against coil current at the pressure of 20 mTorr.

barrier, while the depletion of high-energy electrons tail is caused by the inelastic electron-neutral collisions, such as excitations and ionizations. At H mode, that is, with coil current equal to and larger than 25 A, the two-temperature Maxwellian EEDF in the elastic collision energy range, that is, less than 11.56 eV (the excitation threshold), now disappears due to high electron density and frequent collisions, and the high-energy electrons' depletion via inelastic collisions still exists because the electron density is not high enough for the e–e Coulomb collisions thermalizing these two electron swarms [17, 18].

In a word, the hybrid model successfully captures the main characteristics of plasma parameters during the mode transition, including both the macroscopic plasma properties and microscopic electron kinetics, and all these predictions presented here agree well with the experimental measurements.

2.2. Behavior of metastable neutrals

The behavior of metastable neutrals during the mode transition is investigated by the above hybrid model, with the advanced reaction set that includes the metastables and all relevant reactions [19]. In **Figure 9**, the metastable densities, sampled at the discharge center, versus applied power at different pressures are presented. The densities at low and high pressures, that is, 30 and 300 mTorr, both first increase and then decrease with the power, and the decreasing trend at high pressure is more obvious. Hence, the metastables density increases with power at E mode while decreases with power at H mode, which is different with the electron density trend in Section 2.1. In **Figure 10**, the metastables density profiles at different

http://dx.doi.org/10.5772/intechopen.76654

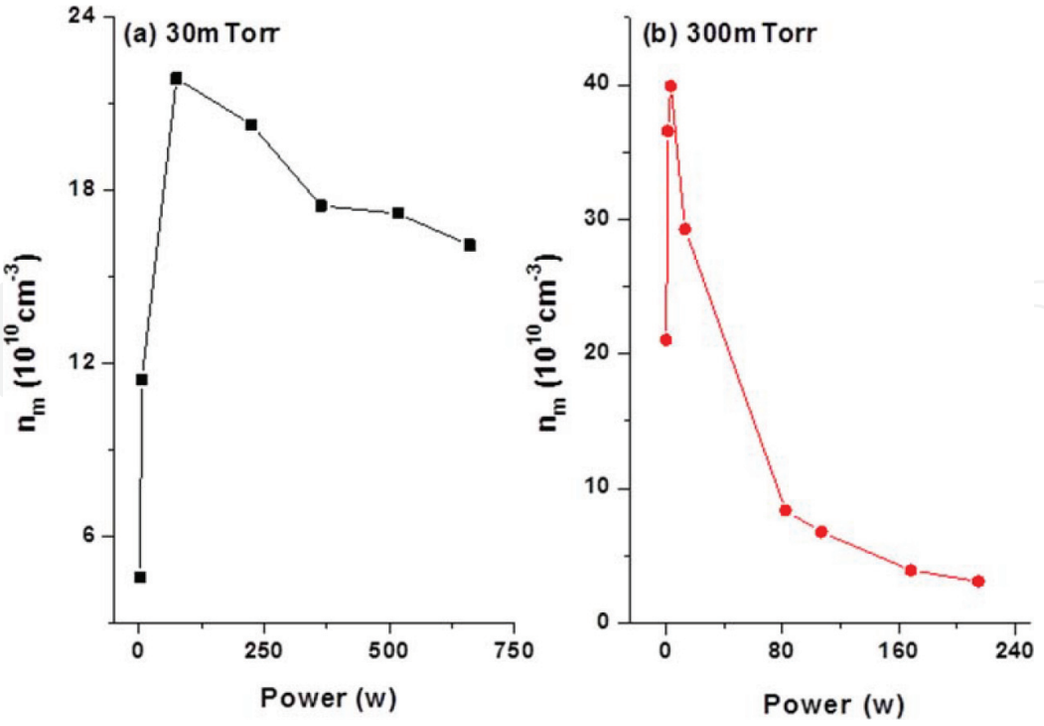

Figure 9. Metastables densities, sampled at the discharge center, versus power at different pressures.

coil currents are presented. It is shown that the peak density keeps increasing with coil current, however, the peak location basically shifts from the discharge center at E mode toward the coil at H mode, thus leading to the non-monotonic varying trends of metastables' densities at the discharge center in **Figure 9**. The localizing trend of metastables density to the coil with coil current is caused by the fact that multistep ionization becomes more and more important as the plasma density is increased, to an extent when the negative source, that is, multistep ionization rate larger than the excitation rate, is formed. The stationary metastables continuity equation with a negative source can be characterized as Bessel's equation with imaginary argument that shows spatial characteristics analogous to the localized profile. This localizing effect is more important at high pressure due to the prevalence of multistep ionizations; hence, the decreasing trend of metastables density with power is more obvious at high pressures. Last, the model predicted a non-monotonic variation of metastables density during mode transition which agrees well with the experiment [20].

Besides the exploration of metastables evolution along with mode transition, the role of metastables in determining the hysteresis is still investigated through the hybrid model. The behind mechanisms that generate hysteresis are difficultly identified since it is a process that is interplayed by so many elements. In the literature, many papers ascribed the hysteresis to the multistep ionizations [13, 21]. To assess this argument, in **Figure 11**, the influence of metastables on electron density and temperature variations versus power is presented. Inclusion of metastables and multistep ionization overall elevates electron densities and meanwhile reduces electron temperatures against the power; however, it does not trigger hysteresis. Besides, the metastables change the trend of electron temperature with power at the H mode.

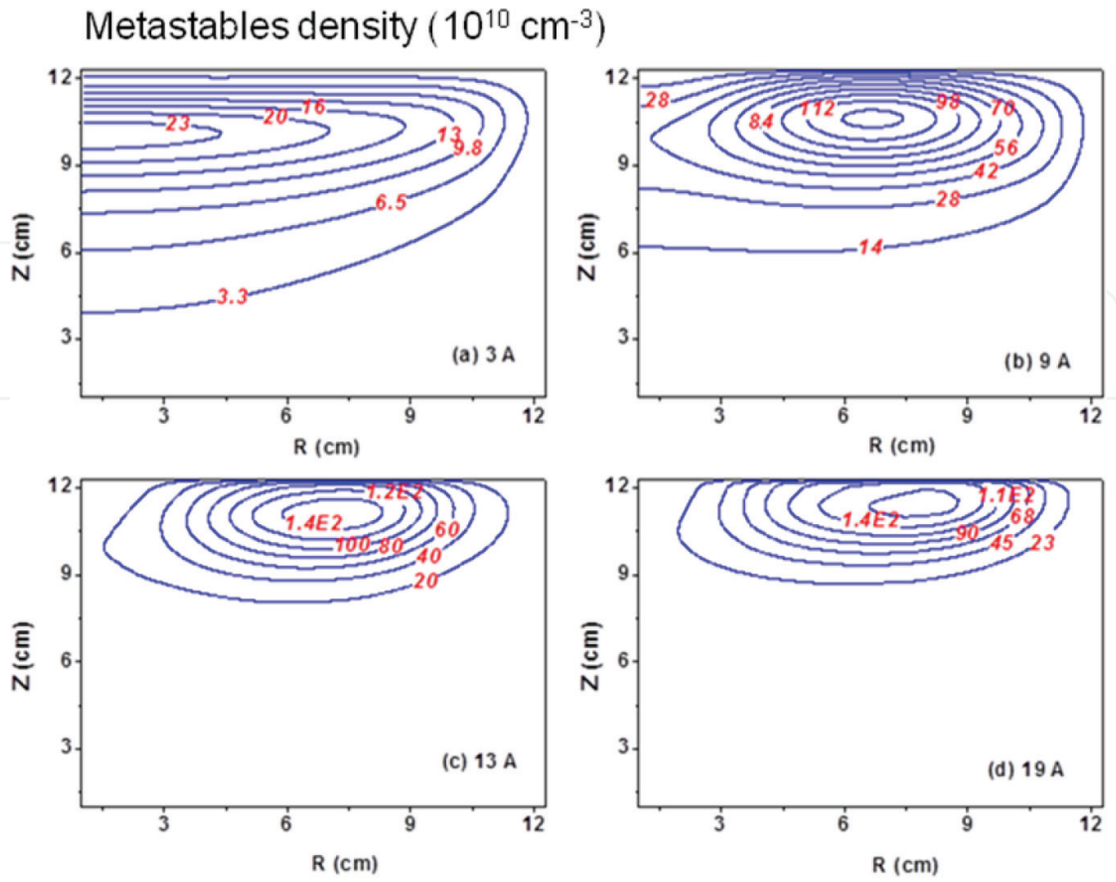

Figure 10. Metastables density profiles at different coil currents at the pressure of 100 mTorr.

The decrease of temperature with power when including metastables is caused by the fact that ionizations consume electron kinetic energy more effectively than excitations, as revealed by a novel electron mean energy Equation [22].

2.3. Discontinuous mode transition and hysteresis excited by matching network

The discontinuity feature of mode transition and interesting hysteresis phenomena have attracted people's attention for years. They are easily observed in the experiments [16, 23] and can be analytically predicted by stationary zero-dimensional global model [24, 25]. However, it is difficult for the self-consistent multidimensional models to capture the discontinuity and hysteresis unless the external circuit module is taken into account. In this chapter, the conventional fluid model that describes the pure inductive mode is extended by including the capacitive mode and advanced by introducing an equivalent circuit module [26, 27]. The diagram of equivalent circuit is illustrated in **Figure 12**. It consists of radio frequency (RF) power source, matching network that consists of parallel and series capacitors and capacitive and inductive coupling branches. The capacitive coupling components include dielectric window capacitor, sheath transferred capacitor and bulk plasma-transferred resistance. The inductive coupling branch is actually based on a transformer model [13], where the coil itself and plasma-transferred inductor and resistor are included and the relations between the coil and plasma-transferred

http://dx.doi.org/10.5772/intechopen.76654

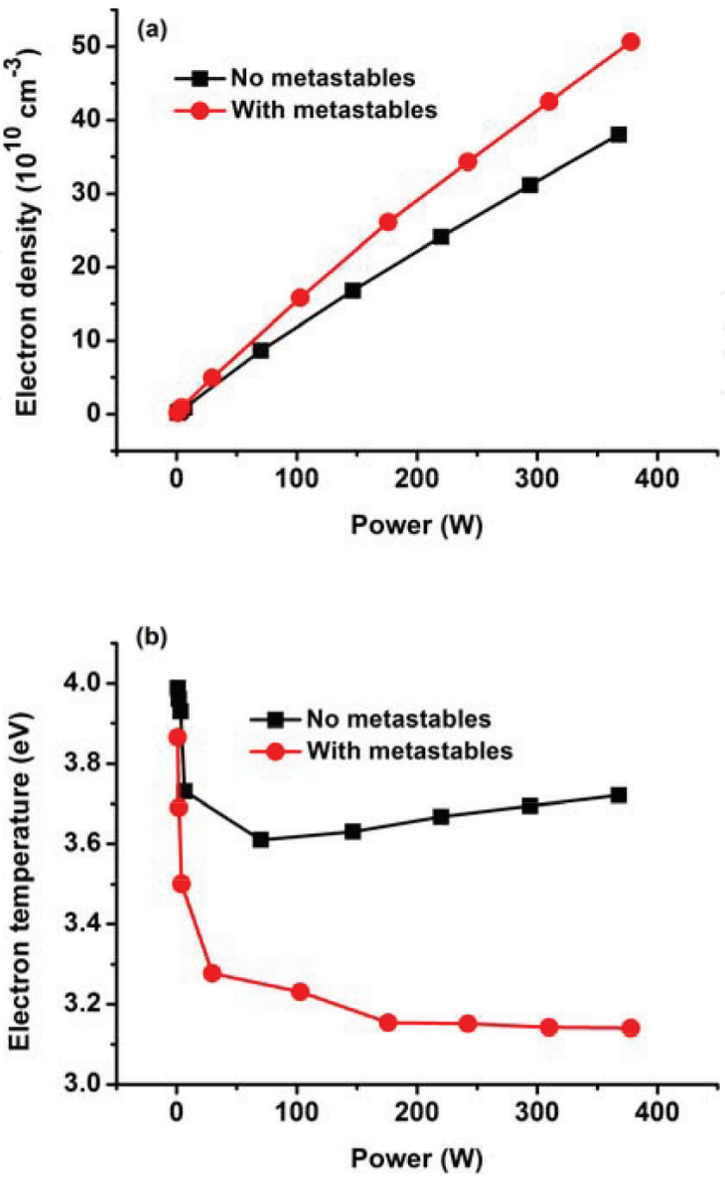

Figure 11. Electron densities (a) and temperatures (b) versus power at two cases, i.e., (1) no metastables and (2) with metastables in the model.

impedances are illustrated in the square of **Figure 12**. The plasma resistances in the capacitive and inductive branches are both transferred through the Ohm's heating mechanism but the capacitive resistance is based on radial and axial plasma current components [3] and the inductive resistance on the azimuthal current component [28].

Via the circuit module, the coil current and voltage, boundary conditions for the electromagnetic module to calculate fields can be given through Kirchhoff's law. More importantly, after considering the circuit module the discontinuity of mode transition and hysteresis can be captured by a fluid model since the mutual interacting details between the circuit and plasma, probably nonlinear, are contained. Of more significance is that two excitation means of mode transitions that have widely been seen in experiments, that is, by means of varying power

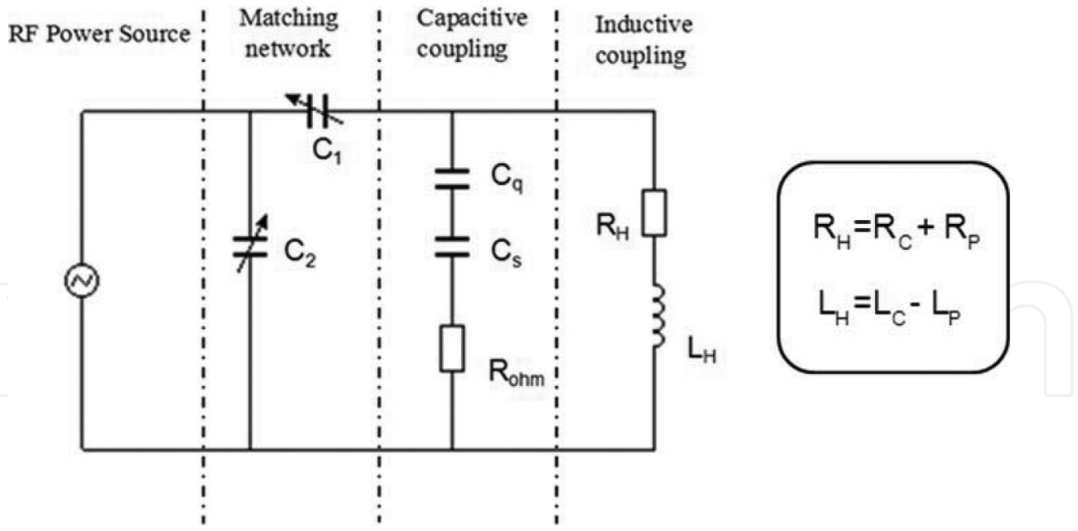

Figure 12. Components of equivalent circuit module.

[16, 23] and matching network [29], can be both captured by this advanced fluid model that couples an external circuit module.

In **Figure 13**, the discontinuous mode transition at a low pressure of 20 mTorr and hysteresis at high pressure of 100 mTorr is perfectly generated by the fluid model, via the alteration of electron density versus series capacitance of matching network. This prediction agrees well with the experimental observations that hysteresis mostly appears at relatively high pressures [21, 23]. Accordingly, the electron temperature just displays mode transition at low pressure, but hysteresis at high pressure, as shown in **Figure 14**. The variations of electron density and temperature with E–H mode transition predicted by the fluid model are in agreement with the hybrid model in Section 2.1.

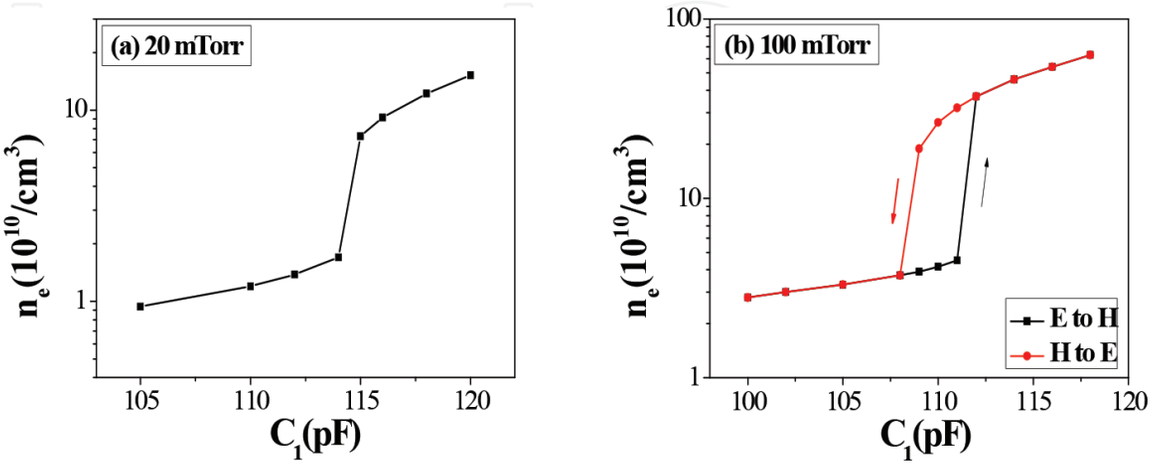

Figure 13. Discontinuous electron density variation versus the series capacitance of matching network at low pressure of 20 mTorr (a) and hysteresis loop of electron density against the series capacitance at high pressure of 100 mTorr.

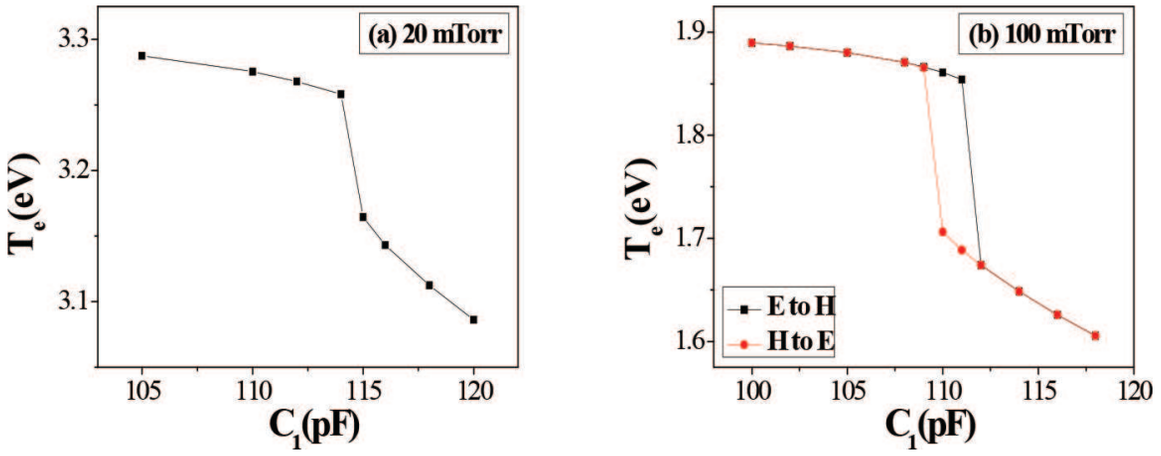

Figure 14. Discontinuous electron temperature variation versus the series capacitance of matching network at low pressure of 20 mTorr (a) and hysteresis loop of electron temperature against the series capacitance at high pressure of 100 mTorr.

Interestingly, the plasma-transferred impedance evolves similarly to the plasma parameters, that is, discontinuously jumping at low pressure and displaying hysteresis at high pressure. In **Figures 15** and **16**, the plasma resistance and inductance of inductive branch and sheath width and capacitance of capacitive branch are plotted against the series capacitance, respectively, at the high pressure of 100 mTorr. In **Figure 15**, at the E–H mode transition, the plasma resistance and inductance both increase because of high-plasma density and strong azimuthal current density. The high-plasma inductance at the H mode weakens the system inductance according to the formula in **Figure 12**, as determined by the law of electromagnetic induction. In **Figure 16**, the sheath width significantly decreases with E–H mode transition due to the scaling law [6] and the sheath transferred capacitance, inversely proportional to mean sheath width, increases substantially. At the H–E mode transition of the hysteresis loop, the opposite cases happen.

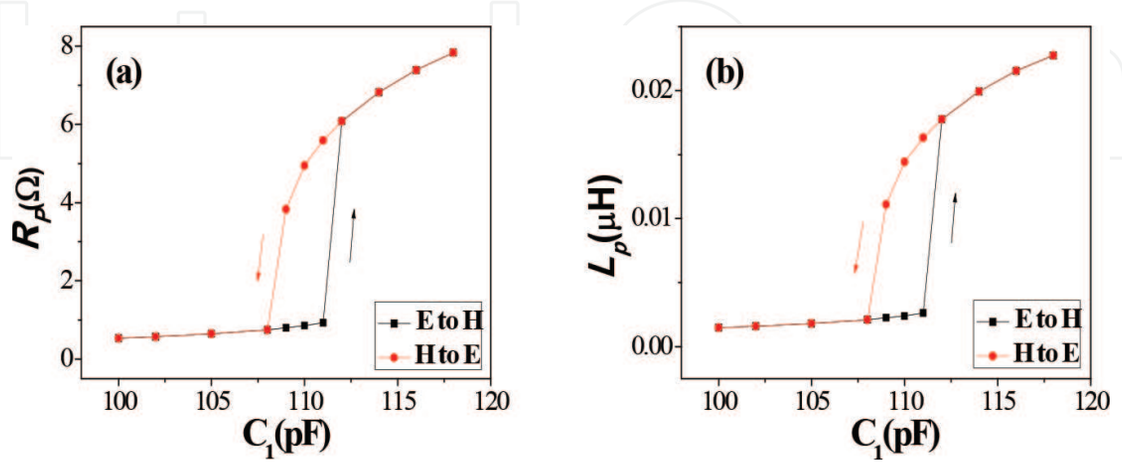

Figure 15. Variations of plasma-transferred resistance (a) and inductance (b) of the inductive branch of equivalent circuit in the hysteresis loop at high pressure of 100 mTorr.

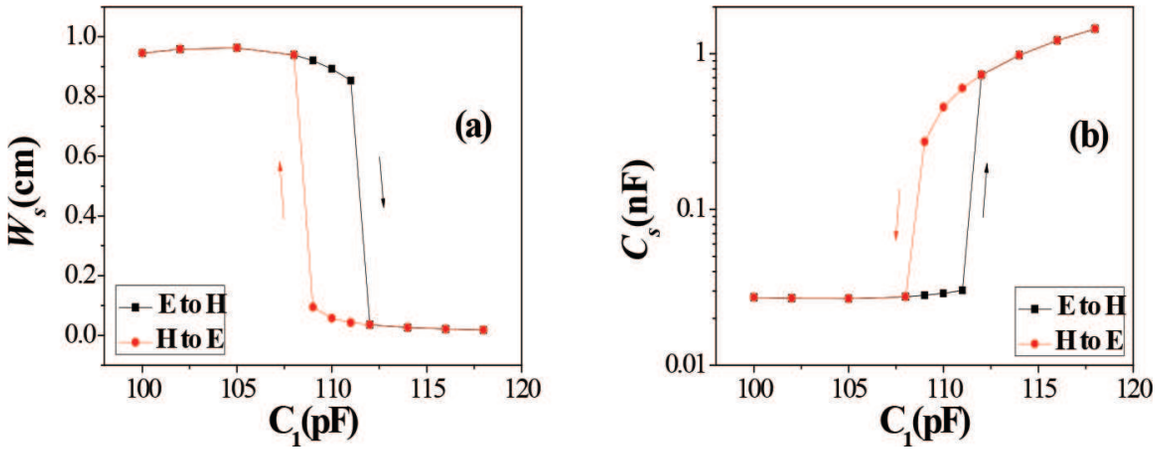

Figure 16. Variations of sheath width (a) and transferred sheath capacitance (b) in the hysteresis loop at high pressure of 100 mTorr.

3. Conclusion and further remarks

The low-pressure radio frequency ICP source is characterized as non-equilibrium, weakly ionized and bounded plasma and finds wide applications in many fields. It holds many interesting physical phenomena and mechanisms. One is the mode transition and hysteresis that happen at two operating modes, that is, inductive and capacitive modes. In this chapter, the characteristics of plasma parameters and neutrals during mode transition are presented by a hybrid model. Moreover, the discontinuity feature of mode transition and hysteresis excited by adjusting the matching network are predicted by a fluid model that couples an external equivalent circuit module. Still, the role of metastables on triggering hysteresis is discussed and the interesting hysteresis loop formed by plasma-transferred impedance is analyzed. The present chapter indicates that the mutual interaction of plasma with circuit is the reason which excites the hysteresis.

Note that the mode transitions and hysteresis of ICP sources are very complicated. Besides the above representative features, it still exhibits research values in the topics of reactive gas mixtures, such as O_2 [30], CF_4/Ar [31], SO_2 [32], ammonia [33] and so on and double hysteresis loop [29], inverse hysteresis [34], spatial characteristics [35], optical emission [36], electrical diagnostics [37], instability of electronegative plasma source [38] and so on. To the author, the exploration of precursors that triggers hysteresis, for instance, metastables and multistep ionizations [13, 21], electron energy distribution function [39], power coupling efficiency [40], sheath [24, 41], external circuit [26, 27] and nonlinear mechanisms [13] and so on, is the most attractive topic. The investigations greatly advance the improvements of analytical theory, numerical modeling, and experimental diagnostics of low-temperature plasma physics.

Acknowledgements

Gratitude is given due to the support by National Natural Science Foundations of China (Grant No. 11305023), and the useful discussions with Hui-Jing Xu are especially acknowledged.

Author details

Shu-Xia Zhao

Address all correspondence to: zhaonie@dlut.edu.cn

Dalian University of Technology, Dalian, China

References

[1] Adamovich I, Baalrud SD, Bogaerts A, Bruggeman PJ, Cappelli M, Colombo V, Czarnetzki U, Ebert U, Eden JG, Favia P, Graves DB, Hamaguchi S, Heiftje G, Hori M, Kaganovich ID, Kortshagen U, Kushner MJ, Mason NJ, Mazouffre S, Mededovic Thagard S, Metelmann HR, Mizuno A, Moreau E, Murphy AB, Neimira BA, Oehrlein GS, Petrovic ZL, Pitchford LC, Pu YK, Rauf S, Sakai O, Samukawa S, Starikovskaia S, Tennyson J, Terashima K, Turner MM, van de Sanden MCM, Vardelle A: The 2017 plasma roadmap: Low temperature plasma science and technology. Journal of Physics D: Applied Physics 2017;**50**:323001. DOI: 10.1088/1361-6463/aa76f5

[2] Zhao SX, Xu X, Li XC, Wang YN. Fluid simulation of the E-H mode transition in inductively coupled plasma. Journal of Applied Physics. 2009;**105**:083306. DOI: 10.1063/1.311 2009

[3] Chabert P, Braithwite N. Physics of Radio-Frequency Plasmas. New York: Cambridge University Press; 2011.17p

[4] Bittencourt JA. Fundamentals of Plasma Physics. 3rd ed. Berlin/Heidelberg/New York: Springer-Verlag; 2004.580p

[5] Tennyson J, Rahimi S, Hill C, Tse L, Vibhakar A, Akello-Egwel D, Brown DB, Dzarasova A, Hamilton JR, Kaksch D, Mohr S, Wren-Little K, Bruckneier J, Agarwal A, Bartschat K, Bogaerts A, Booth JP, Goeckner MJ, Hassouni K, Itikawa Y, Graams BJ, Krishnakumar E, Laricchiuta A, Mason NJ, Pandey S, Petrovic ZL, Pu YK, Ranjan A, Rauf S, Schulze J, Turner MM, Ventzek P, Whitehead JC, Yoon JS. QDB: A new database of plasma chemistries and reactions. Plasma Sources and Science Technology. 2017;**26**:055014. DOI: 10.1088/1361-6595/aa6669

[6] Lieberman MA, Lichtenberg AJ. Principles of Plasma Discharges and Materials Processing. 2nd ed. New York: Wiley-Interscience; 2005.387p

[7] Economou DJ. Pulsed plasma etching for semiconductor manufacturing. Journal of Physics D: Applied Physics. 2014;**47**:303001. DOI: 10.1088/0022-3727/47/30/303001

[8] Lee SH, Cho JH, Huh SR, Kim GH. Standing wave effect on plasma distribution in an inductively coupled plasma source with a short antenna. Journal of Physics D: Applied Physics. 2014;**47**:015205. DOI: 10.1088/0022-3727/47/1/015205

[9] Si XJ, Zhao SX, Xu X, Bogaerts, Wang YN. Fluid simulations of frequency effects on nonlinear harmonics in inductively coupled plasma. Physics of Plasmas. 2011;**18**:033504. DOI: 10.1063/1.3566007

[10] Mishra A, Kim TH, Kim KN, Yeom GY. Mass spectrometric study of discharges produced by a large-area dual-frequency-dual-antenna inductively coupled plasma source. Journal of Physics D: Applied Physics. 2012;**45**:475201. DOI: 10.1088/0022-3727/45/47/475201

[11] Tyshetskiy YO, Smolyakov AI, Godyak VA. Reduction of electron heating in the low-frequency anomalous-skin-effect regime. Physical Review Letters. 2003;**90**:255002. DOI: 10.1103/PhysRevLett.90.255002

[12] Hagelaar GJM. Fluid description of non-local electron kinetics in inductively coupled plasmas. Plasma Sources Science and Technology. 2008;**17**:025017. DOI: 10.1088/0963-0252/17/2/025017

[13] Turner MM, Lieberman MA. Hysteresis and the E-to-H mode transition in radiofrequency inductive discharges. Plasma Sources Science and Technology. 1999;**8**:313-324. DOI: 10.1088/0963-0252/17/2/025017

[14] Zhao SX, Gao F, Wang YN. Dynamic investigation of mode transition in inductively coupled plasma with a hybrid mode. Journal of Physics D: Applied Physics. 2009;**42**:225203. DOI: 10.1088/0022-3727/42/22/225203

[15] Godyak VA, Piejak RB. Abnormally low electron energy and heating-mode transition in a low-pressure argon rf discharge at 13.56MHz. Physical Review Letters. 1990;**65**:996-999

[16] Ostrikov KN, Xu S, Yu MY. Power transfer and mode transitions in low-frequency inductively coupled plasmas. Journal of Applied Physics. 2000;**88**:2268-2271

[17] Gao F, Zhao SX, Li XS, Wang YN. Comparison between experiment and simulation for argon inductively coupled plasma. Journal of Applied Physics. 2000;**88**:2268-2271

[18] Vasenkov A, Kushner MJ. Electron energy distributions and anomalous skin effects in high-plasma-density inductively coupled discharges. Physical Review E. 2002;**66**:066411

[19] Zhao SX, Wang YN. Investigation of the effect of metastable atoms on mode transition in argon inductive discharge via a hybrid model. Journal of Physics D: Applied Physics. 2010;**43**:275203. DOI: 10.1088/0022-3727/43/27/275203

[20] Daltrini AM, Moshkalev SA, Morgan TJ, Piejak RB, Graham WG. Plasma power measurement and hysteresis in the E-H transition of a rf inductively coupled plasma system. Applied Physics Letters. 2008;**92**:061504. DOI: 10.1063/1.2844885

[21] Lee MH, Lee KH, Hyun DS, Chung CW. On the hysteresis in E to H and H to E transitions and the multistep ionization in inductively coupled plasma. Applied Physics Letters. 2007;**90**:191502. DOI: 10.1063/1.2734501

[22] Zhao SX. Non-monotonic behavior of electron temperature in argon inductively coupled plasma and its analysis via novel electron mean energy equation. Physics of Plasmas. 2018;**25**(3):033516

[23] Daltrini AM, Moshkalev SA, Monteiro MJR, Besseler E, Kostryukov A, Machia M. Mode transitions and hysteresis in inductively coupled plasmas. Journal of Applied Physics. 2007;**101**:073309. DOI: 10.1063/1.2715845

[24] EI-Fayoumi IM, Jones IR, Turner MM. Hysteresis in the E- to H-mode transition in a planar coil, inductively coupled RF argon discharge. Journal of Physics D: Applied Physics. 1998; **31**:3082-3094

[25] Lee MH, Chung CW. On the E to H mode and H to E transition mechanisms in inductively coupled plasma. Physics of Plasmas. 2006;**13**:063510. DOI: 10.1063/1.2212387

[26] Xu HJ, Zhao SX, Zhang YR, Gao F, Li XC, Wang YN. Equivalent circuit effects on mode transitions in H_2 inductively coupled plasmas. Physics of Plasmas. 2015;**22**:043508. DOI: 10.1063/1.4917335

[27] Xu HJ, Zhao SX, Gao F, Zhang YR, Li XC, Wang YN. Discontinuity of mode transition and hysteresis in hydrogen inductively coupled plasma via a fluid model. Chinese Physics B. 2015;**24**:115201. DOI: 10.1088/1674-1056/24/11/115201

[28] EI-Fayoumi IM, Jones IR. The electromagnetic basis of the transformer model for an inductively coupled RF plasma source. Plasma Sources Science and Technology. 1998;**7**: 179-185

[29] Gao F, Zhao SX, Li XS, Wang YN. Effects of matching network on the hysteresis during E and H mode transitions in argon inductively coupled plasma. Physics of Plasmas. 2010;**17**: 103507. DOI: 10.1063/1.3496385

[30] Wegner T, Küllig C, Meichsner J. On the E-H transition in inductively coupled radio frequency oxygen plasmas: I. Density and temperature of electrons, ground state and singlet metastable molecular oxygen. Plasma Source Science and Technology. 2017;**26**: 025006. DOI: 10.1088/1361-6595/26/2/025006

[31] Liu W, Gao F, Zhao SX, Li XC, Wang YN. Mode transition in CF_4+Ar inductively coupled plasma. Physics of Plasmas. 2013;**20**:123513. DOI: 10.1063/1.4858900

[32] Zaplotnic R, Vesel A, Mozetic M. Investigation of reactive plasma species created in SO_2 by an inductively coupled RF discharge in E- and H- mode. Journal of Applied Physics. 2016;**120**:163302. DOI: 10.1063/1.4966171

[33] Draskovic-Bracun A, Mozetic M, Zaplotnik R. E- and H-mode transition in a low pressure inductively coupled ammonia plasma. Plasma Processes and Polymers. 2018;**15**:e1700105. DOI: 10.1002/ppap.201700105

[34] Lee MH, Chung CW. Observation of inverse hysteresis in the E to H mode transitions in inductively coupled plasmas. Plasma Source Science and Technology. 2010;**19**:015011. DOI: 10.1088/0963-0252/19/1/015001

[35] Lee HC, Kim YC, Chung CW. Evolution of two-dimensional plasma density on the E-H heating mode transition in planar type inductively coupled plasma. IEEE Transactions on Plasma Science. 2011;**39**:2536-2537. DOI: 10.1109/TPS.2011.2135382

[36] Morishita S, Hayashi Y, Makabe T. Spatiotemporal optical structure of plasmas in the E-to-H transition in an inductively coupled plasma in Ar. Plasma Source Science and Technology. 2010;**19**:055007. DOI: 10.1088/0963-0252/19/5/055007

[37] Lee HC, Chung CW. Comparisons of the electrical characteristics by impedance matching conditions on the E-H and H-E transition and the hysteresis of inductively coupled plasma. Thin Solid Films. 2012;**521**:185-188. DOI: 10.1016/j.tsf2011.12.015

[38] Corr SC, Steen PG, Graham WG. Instabilities in an inductively coupled oxygen plasma. Plasma Source Science and Technology. 2003;**12**:265-272

[39] Lee HC, Chung CW. Effect of electron energy distribution on the hysteresis of plasma discharge: Theory, experiment and modeling. Scientific Reports. 2015;**5**:15254. DOI: 10.1038/srep15254

[40] Suzuki K, Nakamura K, Ohkubo H, Sugai H. Power transfer efficiency and mode jump in an inductive RF discharge. Plasma Source Science and Technology. 1998;**7**:13-20

[41] Cunge G, Crowley B, Vender D, Turner MM. Characterization of the E to H transition in a pulsed inductively coupled plasma discharge with internal coil geometry: Bi-stability and hysteresis. Plasma Source Science and Technology. 1999;**8**:576-586